RSC Advances

PAPER

View Article Online
View Journal | View Issue

Check for updates

Cite this: *RSC Adv.*, 2021, **11**, 34589

Completely green synthesis of rose-shaped Au nanostructures and their catalytic applications†

Jae Hwan Jeong,[a] Astrini Pradyast,[a] Hyeonbo Shim,[a] Hee-Chul Woo[b] and Mun Ho Kim *[a]

The importance of and demand for eco-friendly syntheses of metal nanocrystals are increasing. In this study, a novel protocol for the one-pot, template/seed-free, and completely green synthesis of rose-shaped Au nanostructures with unique three-dimensional hierarchical structures was developed. The synthesis of the nanostructures was carried out at room temperature using water as a reaction medium and an eco-friendly biopolymer (sodium salt of alginic acid (Na-alginate)) as a reducing agent. The morphologies of the Au nanostructures were controlled by adjusting the amount of capping ligand (polyvinylpyrrolidone (PVP)) in the reaction mixture, and a limited ligand protection (LLP) strategy was used to induce the formation of rose-shaped Au nanostructures. A formation mechanism for the rose-shaped Au nanostructures was proposed on the basis of structural characterizations and the shape evolution of the nanostructures. The unique structural features of the rose-shaped nanostructures, which include a high surface roughness, a large surface area-to-volume ratio, and abundant edges and sharp tips, motivated us to use them as a high-performance catalyst. They were used as an environmentally benign catalyst in an organic reaction to remove a hazardous chemical from an aqueous medium: specifically, the hydrogenation of 4-nitrophenol (4-NP) to 4-aminophenol (4-AP) by sodium borohydride. Without an additional supporting material, the rose-shaped Au nanostructures showed outstanding catalytic activity that was maintained when the catalyst was recycled and used a total of five times.

Received 10th September 2021
Accepted 18th October 2021

DOI: 10.1039/d1ra06805a

rsc.li/rsc-advances

Open Access Article. Published on 26 October 2021. Downloaded on 1/16/2025 9:05:36 AM.
This article is licensed under a Creative Commons Attribution-NonCommercial 3.0 Unported Licence.

Introduction

Because the chemical and physical properties of gold (Au) nanocrystals depend heavily on their size and shape, the size- and shape-controlled synthesis of Au nanocrystals is an important topic.[1,2] The literature includes numerous reports of the synthesis of Au nanocrystals with various shapes, including zero-dimensional (0D, such as spheres and platonic shapes),[3,4] one-dimensional (1D, such as rods and nanowires),[5,6] two-dimensional (2D, such as plates and sheets),[7,8] and three-dimensional (3D, such as multipods and nanocages).[9,10] Among the various reported structures, Au nanocrystals with 3D hierarchical structures such as flower-like architectures have attracted considerable attention because of their unique structural features, which include a high surface roughness, a large surface area-to-volume ratio, and abundant edges and sharp tips.[11–18] These unique features enable these nanocrystals to be used as advanced and high-performance materials, particularly catalysts.[19–21] Several synthesis strategies for synthesizing Au nanostructures with flower-like architectures have been reported, including a soft template method,[18] hard template method,[21] electrochemical methods,[15,22] a galvanic replacement reaction,[23] and seeded-growth syntheses.[24,25] Because these approaches require the preparation of complex templates or seeds in advance and tend to involve time-consuming, complicated, or costly processes, the development of a one-pot, easy-to-implement method for preparing Au nanostructures with 3D hierarchical structures is still highly desirable and technically important.

The challenge in developing a novel synthesis method for noble-metal nanocrystals is the adoption of a "green" approach that reduces the use of organic solvents and reagents that are potentially hazardous to both the environment and human health.[26,27] The use of an eco-friendly solvent system and natural resources is critical to achieving this goal.[28] Water, the most commonly accessible solvent on Earth, has long been considered a safe, nontoxic, environmentally benign, and ideal solvent system for syntheses.[29] Bio-sourced materials, including biopolymers, are candidates for environmentally benign reducing and stabilizing agents for the synthesis of noble-metal nanocrystals.[30] The adoption of energy-saving experimental conditions that do not require high energy input or high

[a]*Department of Polymer Engineering, Pukyong National Univeristy, 45 Yongso-ro, Nam-gu, Busan 48513, Republic of Korea. E-mail: munho@pknu.ac.kr*

[b]*Department of Chemical Engineering, Pukyong National University, 45 Yongso-ro, Nam-gu, Busan 48513, Republic of Korea*

† Electronic supplementary information (ESI) available. See DOI: 10.1039/d1ra06805a

© 2021 The Author(s). Published by the Royal Society of Chemistry

Open Access Article. Published on 26 October 2021. Downloaded on 1/16/2025 9:05:36 AM.
This article is licensed under a Creative Commons Attribution-NonCommercial 3.0 Unported Licence.

pressures is also an important factor in the green synthesis of noble-metal nanocrystals.[31,32] However, substantial barriers must be overcome to realize the size- and shape-controlled synthesis of noble metals *via* completely green approaches.

The catalytic conversion of small organic molecules to value-added products under ambient conditions is an attractive topic.[33,34] In particular, catalysts in water are important in the sustainable design of organic-compound-conversion reactions because of their reduced cost and reduced environmental impact compared with organic-solvent-based reactions.[35–37] 4-Nitrophenol (4-NP), which is widely used in medicaments, dyes, plastics, pesticides, and anticorrosive agents, has been identified as one of the most dangerous and toxic pollutants.[38–40] Therefore, the hydrogenation reaction of 4-NP by sodium borohydride ($NaBH_4$) to 4-aminophenol (4-AP) is potentially an effective and eco-friendly method to remove 4-NP from water because 4-AP is an important intermediate chemical used in many industries and is also easier to mineralize and remove from waste streams than 4-NP.[41–43] Because the hydrogenation of 4-NP to 4-AP by $NaBH_4$ takes several days, a stable and efficient catalyst is needed to dramatically reduce the reaction time.[44,45]

In the present study, we report a facile, green and low-cost synthetic method for producing rose-shaped Au nanostructures with unique 3D hierarchical structures. This new synthesis route differs from and has several advantages over previously reported methods for synthesizing Au nanostructures with flower-like structures. First, it follows an easy-to-use protocol based on a one-pot synthesis method that does not require multistep growth processes such as the preparation of complex templates or seeds in advance. Second, the synthetic procedures involve environmentally acceptable "green" chemistry. In the proposed method, only water was used as a reaction medium in all of the reactions and no additional toxic organic solvents were required. In addition, the sodium salt of alginic acid (Na-alginate), an eco-friendly biopolymer based on brown algae extract,[46,47] was used as a reducing agent. Because the polyvinylpyrrolidone (PVP) used as a capping ligand is also nontoxic and biocompatible,[48] the process does not involve any toxic substances. Moreover, it is a low-cost protocol, being based on a room-temperature process. The room temperature procedure is advantageous for commercial applications because of its low power consumption and no inconvenience of handling special equipment. Although we achieved a substantial reduction in reaction time (within 3 h), the synthetic results were still reproducible. Rose-shaped Au nanostructures with unique 3D hierarchical structures were synthesized by simply adding a $HAuCl_4$ aqueous solution to an aqueous solution containing Na-alginate and PVP. Here, a limited ligand protection (LLP) growth strategy controlled by the amount of capping ligand (PVP) was used to induce the 3D stacking of Au nanoplates.

The rose-shaped Au nanostructures synthesized in the present study were used as eco-friendly and effective catalysts in the hydrogenation of 4-NP to 4-AP by $NaBH_4$ in water. The prepared nanostructures showed excellent catalytic activity because of their high surface roughness, large surface-to-volume ratio, and abundant edges and sharp tips resulting from their highly nanotextured topography and layered structure. The relatively large particle size, which reached several hundred nanometers, and three-dimensionally stacked structures with numerous layers enabled their easy separation from the reaction mixture by simple centrifugation after the catalytic reaction; they can therefore be used as high-performance catalysts without a supporting material. They showed excellent recyclability, exhibiting only slight degradation of their catalytic performance over five cycles.

Experimental

Chemicals and materials

Na-alginate, PVP ($M_w \approx 360$ kDa), gold(III) chloride trihydrate ($HAuCl_4$), 4-NP, and $NaBH_4$ were purchased from Sigma-Aldrich. The deionized (DI) water used in all reactions was purchased from SK Chemical (Republic of Korea). All reagents were of analytical grade and were used as supplied, without further purification.

Synthesis of rose-shaped Au nanostructures

In a typical synthesis, 2 mL of 0.5 wt% Na-alginate aqueous solution, 1 mL of 0.05 wt% PVP (360 kDa), and 4 mL of DI water were added to a 20 mL glass vial (liquid scintillation vial with a polyethylene liner and a white cap, Research Product International Corp.) and mixed with a vortex for 10 s. 1 mL of 7 mM $HAuCl_4$ aqueous solution was then rapidly added to the vial using a glass pipette. The synthesis reaction was carried out at room temperature under ultraviolet (UV) irradiation using a UV-light curing system with a UVA (mainly 365 nm) output of 6 W cm^{-2}. After 1.5 h of UV irradiation, the bright-yellow reaction medium became colorless. As the reaction progressed, the color of the reaction solution, which was initially bright yellow, changed to blue and was dark-blue when the reaction was completed after 3 h. To adjust the reduction kinetics, other series of the reactions were run by adding different amounts of PVP (the PVP-to-$HAuCl_4$ weight ratio: from 0 to 18) or varying the concentration of $HAuCl_4$. The reaction product was collected by centrifugation at 6000 rpm for 10 min, washed five times using DI water, and finally dispersed and stored in DI water for further experiments.

Hydrogenation of 4-NP to 4-AP by reaction with $NaBH_4$

The hydrogenation of 4-NP to 4-AP by $NaBH_4$ was carried out at room temperature in a quartz cuvette. $NaBH_4$ (700 mM) aqueous solution was prepared and placed in a refrigerator. An aqueous solution of 4-NP (2.5 μL, 10 mM) was prepared and added to a cuvette containing 1 mL of DI water. 10 μL of the $NaBH_4$ solution (700 mM) were added to a quartz cell to convert the 4-NP to 4-nitrophenolate ion. 100 μL of the aqueous solution containing the rose-shaped Au nanoparticles (~0.06 mg) was then added to the cuvette. The reduction reaction was monitored by UV-Vis spectrophotometry at time intervals of 10 s.

© 2021 The Author(s). Published by the Royal Society of Chemistry

Open Access Article. Published on 26 October 2021. Downloaded on 1/16/2025 9:05:36 AM.
This article is licensed under a Creative Commons Attribution-NonCommercial 3.0 Unported Licence.

Characterizations

Transmission electron microscopy (TEM) observations were carried out using a transmission electron microscope (H-7500, Hitachi) operated at an acceleration voltage of 80 kV. Specimens for TEM observation were prepared by dropping an aqueous solution of Au nanoparticles onto a carbon-coated Cu grid, followed by drying at room temperature. High-resolution TEM (HR-TEM) micrographs were acquired using a field-emission transmission electron microscope (JEM-2100F, Jeol) operated at 200 kV. Scanning electron microscopy (SEM) micrographs were acquired using a field-emission scanning electron microscope (Mira 3LMH, Tescan) operated at 5 kV. X-ray diffraction (XRD) analysis was conducted using a powder X-ray diffractometer (X'Pert3, PANalytical). Thermogravimetric analysis (TGA) was conducted using a Pyris 1 thermogravimetric analyzer (PerkinElmer). UV-Vis spectra were acquired at room temperature using a UV-Vis spectrophotometer (Cary 50, Agilent).

Results and discussion

Synthesis and characterizations of rose-shaped Au nanostructures

In the present study, Au nanostructures were synthesized using a water-based one-step synthesis method in which Na-alginate was used as a reducing and stabilizing agent. PVP was introduced as a capping ligand, and the reaction was carried out at room temperature under UV irradiation for 3 h. As shown in Fig. 1(a), the reaction mixture was initially light-yellow because of the $HAuCl_4$ solution used as a Au precursor; however, the aqueous solution changed to dark-blue after the Au^{3+} ions were reduced by the photochemical reaction. Fig. 1(b) and (c) show SEM images of the synthesized Au nanostructures. Interestingly, the synthesized particles exhibited a rose-shaped structure with numerous stacked plate-shaped layers. The average size of the rose-shaped nanostructures was approximately 430 ± 45 nm. A typical TEM image of the Au nanostructures is shown in Fig. 1(d). The image shows different regions of contrast, where the hierarchical layered structure of the Au nanostructures is easily observed.

To confirm that the synthesis of the rose-shaped Au nanostructures occurred through the photochemical reduction by alginate and UV light, control experiments were performed by excluding a specific reactant from the reaction mixture or by controlling the UV-light irradiation. Fig. S1(a)† shows that the reaction proceeded in the absence of PVP under the same conditions and that it became dark-blue, similar to the mixture shown in Fig. 1(a). These results indicate that the reduction reaction of the Au precursor proceeded in the absence of PVP. Fig. S1(b)† shows that the reaction mixture with Na-alginate excluded; the yellow mixture indicates that the Au precursor was not reduced at all. These experimental results demonstrate that the Na-alginate acts as a reducing agent under the current synthesis conditions. However, UV light was also observed to strongly affect the formation of the Au nanostructures. The reaction mixture containing both Na-alginate and PVP, where the reaction was performed in a dark room under the same conditions, showed no color change (Fig. S1(c)†). Collectively, these results indicate that the Au precursor was reduced only when alginate was present and under irradiation with UV light, confirming the photochemical reduction in the presence of alginate and UV light.

XRD analysis was performed to analyze the crystal nature of the rose-shaped Au nanostructures (Fig. S2†). In the XRD pattern, peaks are observed at 38.4°, 44.5°, 64.8°, and 77.8°; these peaks correspond to the {111}, {200}, {220}, and {311} crystal planes of pure Au, revealing that the rose-shaped nanostructures were composed of Au.[49] However, the peak corresponding to the {111} crystal plane of Au is dominant in the XRD pattern, whereas the intensities of the other peaks are low. This abnormal intensity ratio indicates that the top and bottom surfaces of the plate-layer in the nanostructures consist of {111} facets.[50] HR-TEM was used to gain further insight into the crystal structure of the plate layer (Fig. 2(b)–(d)). The lattice-spacing, separated by 0.25 nm in a hexagonal arrangement, corresponds to 1/3{422} planes of face-centered cubic (fcc) Au, which was mainly observed for thin-film-shaped Au nanocrystals (Fig. 2(d)).[51,52] The corresponding fast Fourier transform (FFT) pattern is shown in the inset of Fig. 2(d). The six diffraction spots with sixfold rotational symmetry confirm that the plate was a single crystal with the {111} crystal plane as its basal plane, consistent with the XRD results.[53] These observations indicate that the rose-shaped nanostructures have multilayered structures of single-crystalline Au nanoplates with the {111} crystal plane at the flat top and bottom surfaces.

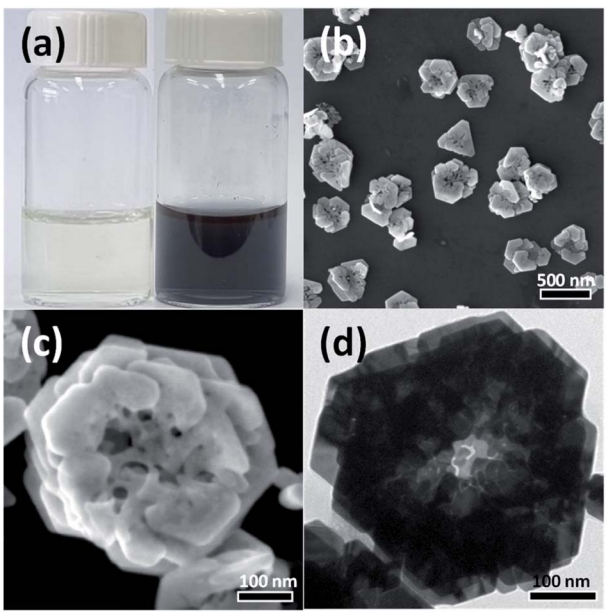

Fig. 1 (a) Photographs of the reaction mixture before (left) and after (right) the UV irradiation process at room temperature for 3 h. (b) Low- and (c) high-magnification SEM images of rose-shaped Au nanostructures. (d) TEM image of the rose-shaped Au nanostructures. In the synthesis, the final concentration of $HAuCl_4$ in the mixture was adjusted to 0.88 mM, and the PVP-to-$HAuCl_4$ weight ratio was 0.18.

Open Access Article. Published on 26 October 2021. Downloaded on 1/16/2025 9:05:36 AM.
This article is licensed under a Creative Commons Attribution-NonCommercial 3.0 Unported Licence.

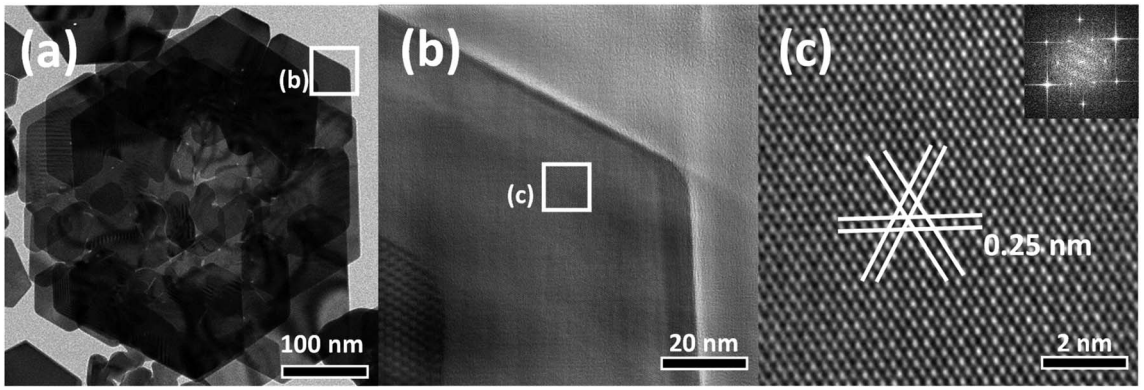

Fig. 2 (a)–(c) HR-TEM images of the rose-shaped Au nanostructures.

The unique structural features of the rose-shaped Au nanostructures, which include a high surface roughness, a large surface area-to-volume ratio, and abundant edges and sharp tips, may make these nanostructures thermodynamically unstable. Thermodynamically unstable nanostructures tend to aggregate or transform during storage in order to reduce their surface energy. In order to evaluate the stability of the rose-shaped Au nanostructures, the final sample dispersed in DI water was aged for at least 3 months at room temperature. As shown in Fig. S3,† the rose-shaped nanostructures obtained in this study maintained their shape for over 3 months of aging and showed no signs of aggregation. That is, despite their unique structural features, the rose-shaped Au nanostructures exhibited high stability with regard to dispersity and shape. This stability, which can be attributed mainly to the PVP that served as a capping ligand, indicates that the rose-shaped Au nanostructures are suitable for real-world applications. Thermogravimetric analysis (TGA) was used to determine the presence and amount of surface-bound ligand coverage on the rose-shaped Au nanocrystals. The residual PVP content as determined by TGA analysis was found to be approximately 3.2 wt% of the final sample mass in the dried state (see Fig. S4†).

Growth mechanism of rose-shaped Au nanostructures

To investigate the growth of the rose-shaped Au nanostructures, we monitored their evolution by stopping the typical synthesis process at different reaction times and observing the Au nanocrystals by TEM. The micrograph of Au nanocrystals obtained at a reaction time of 30 min (Fig. 3(a)) shows that small plate-shaped nanocrystals with a size of 70 nm or less were formed at the early stage of the reaction. The structures evolved to form large plate-shaped particles with abundant edges and tips as their sizes increased to 330 ± 7.89 nm over a period of 1.5 h (Fig. 3(b) and (c)). When the reaction time was further extended to 2 h, new small plate-like particles became stacked on the formed large nanoplates (Fig. 3(d)). After 3 h, as the petal-shaped nanoplates became increasingly stacked, rose-shaped particles were formed and the average size of the rose-shaped particles grew to 430 ± 45 nm (Fig. 3(e)). Changes in the shape and size of the Au nanostructures were clearly observed at reaction times as long as 3 h; however, no substantial changes in shape or size were observed at longer reaction times (Fig. 3(f)). These results suggest that the growth of the rose-shaped nanostructures can be roughly divided into two distinct stages. In the first stage, which corresponds to reaction times shorter than 1.5 h, the nanoplates grow mainly in the lateral dimension and large nanoplates with several edges and tips are formed. In the second stage, corresponding to reaction times beyond 1.5 h, new small plate-shaped particles stack on the top surface of the formed large nanoplates, generating rose-shaped nanostructures.

In the present study, the shape of the Au nanostructures was strongly influenced by the amount of PVP (*i.e.*, capping ligand) in the reaction mixture. Accordingly, an LLP strategy was used to induce the formation of rose-shaped nanostructures. LLP growth strategies have been previously reported for the synthesis of metal or metal oxide nanostructures as a method to induce secondary 3D aggregation of primary nanocrystals by reducing the level of ligand protection.[54–57] When the reaction was carried out only in the presence of Na-alginate without PVP, large 2D structures with amorphous shapes were obtained (Fig. 4(a)). These results indicate that, in the absence of PVP, the formed Au nanoparticles were not stable in the aqueous solution and therefore agglomerated and grew into large particles with amorphous structures. When PVP was introduced and the PVP-to-$HAuCl_4$ ratio was ~0.18, rose-shaped Au nanostructures with stacked plate layers were formed (Fig. 4(b)). In a previous study, the enhanced colloidal stability of the Au nanocrystals in the presence PVP enabled Ag nanocrystals to grow without agglomerating.[48] In addition, PVP is known to stabilize the {111} crystal plane of Au nanocrystals by binding preferentially to the {111} facet over the Au nanocrystals' other facets.[58] Therefore, in the presence of PVP, forming a plate structure having {111} surfaces as top and bottom surfaces is advantageous. However, because the amount of PVP is insufficient, PVP cannot provide adequate protection against crystal growth, which leads to stacking of the as-synthesized nanoplates and to the eventual formation of rose-shaped nanostructures.

The yield of rose-shaped particles in the final product decreased when the PVP-to-$HAuCl_4$ weight ratio was increased to 1.8 (Fig. 4(c)). Because high concentrations of PVP favor

 © 2021 The Author(s). Published by the Royal Society of Chemistry

Open Access Article. Published on 26 October 2021. Downloaded on 1/16/2025 9:05:36 AM.
This article is licensed under a Creative Commons Attribution-NonCommercial 3.0 Unported Licence.

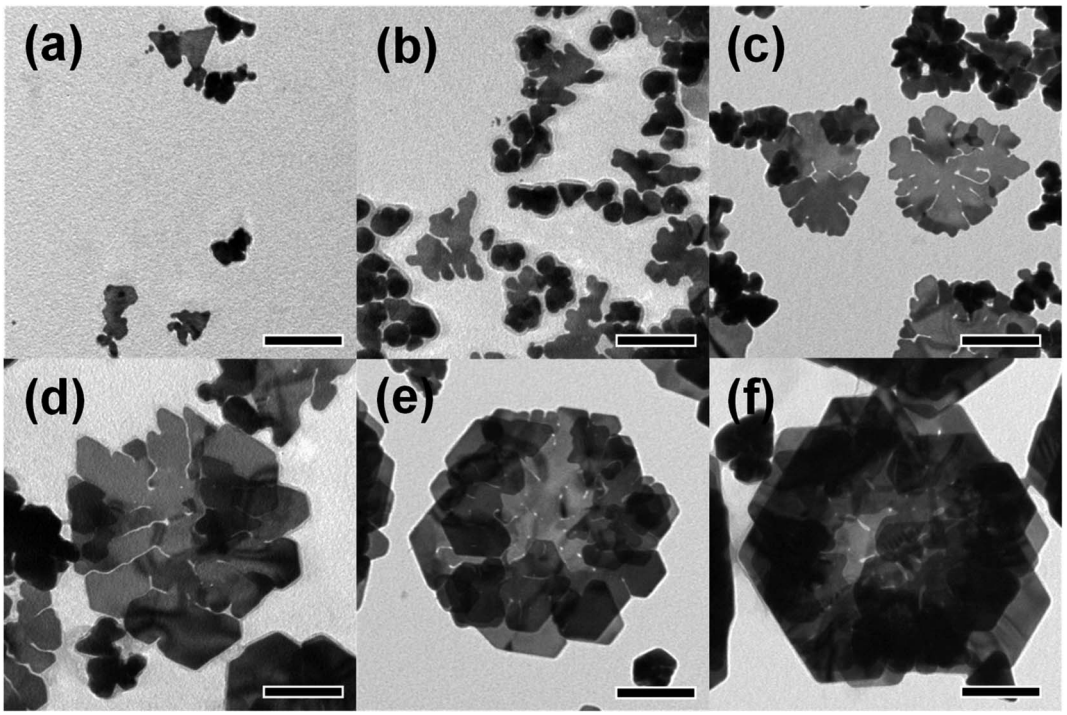

Fig. 3 TEM images of Au nanostructures sampled at different reaction times: (a) 30 min, (b) 1 h, (c) 1.5 h, (d) 2 h, (e) 3 h, and (f) 6 h. The scale bar in each figure represents 100 nm.

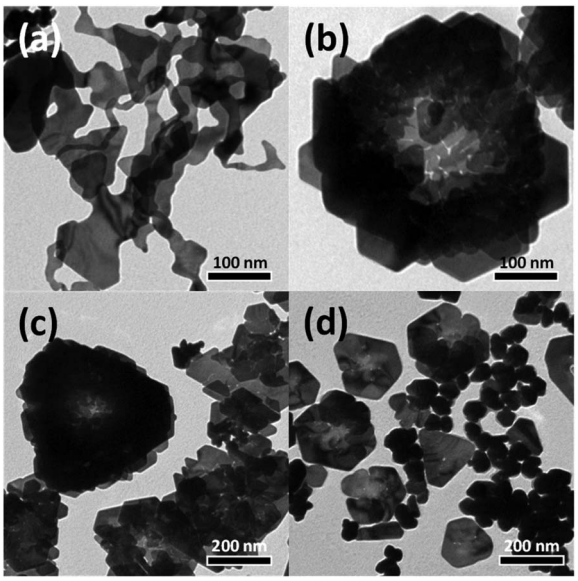

Fig. 4 TEM images of Au nanostructures synthesized using various concentrations of PVP. The PVP-to-$HAuCl_4$ weight ratio was (a) 0, (b) 0.18, (c) 1.8, and (d) 18.

sufficient ligand protection and may interfere with the stacking of the as-synthesized Au nanoplates, Au nanoplates tend to grow individually without stacking, thereby reducing the yield of rose-shaped Au nanostructures in the final product. In addition, the hydroxyl end groups of PVP have sufficient reducing power to reduce the Au precursor.[59] When the PVP-to-$HAuCl_4$ weight ratio was greater than 18, the reducing power of PVP led to the formation of multiply twinned particles reduced by PVP (Fig. 4(d)). To confirm the reduction of the Au precursor by PVP at high PVP concentrations, the reaction was carried out under identical experimental conditions but without Na-alginate, which was used as a reducing agent in the present study. As shown in Fig. S5(a),† when the PVP-to-$HAuCl_4$ weight ratio was 18, Au nanocrystals were produced in the absence of Na-alginate. The Au nanocrystals generated by the reduction of PVP were multiply twinned structures, not plate-shaped (Fig. S5(b) and (c)†), making them similar in shape and size to those shown in Fig. 4(d). Because Au atoms are generated rapidly in the presence of high concentrations of PVP, multiply twinned structures, which are thermodynamically preferred structures, would be obtained.[60] Taken together, these results indicate that the rose-shaped Au nanostructures could be formed in the special reaction region corresponding to LLP, which is highly correlated with the amount of PVP in the reaction mixture. A schematic of the shape change of the Au nanocrystals according to the main reducing agent and colloidal stabilizer is shown in Fig. 5.

On the basis of the experimental results related to the shape evolution of the previously discussed Au nanocrystals, we propose a mechanism for the formation of rose-shaped Au nanostructures. At the early stage of the reaction, small Au nanoplates are formed (Fig. 3(a)). These anisotropic nanostructures are known to dominantly form when Au nanocrystals are formed under mild reducing power.[61] Because the reducing power of Na-alginate is low at room temperature, such plate-like nanostructures are formed at the early stage of the reaction.[45]

Open Access Article. Published on 26 October 2021. Downloaded on 1/16/2025 9:05:36 AM.
This article is licensed under a Creative Commons Attribution-NonCommercial 3.0 Unported Licence.

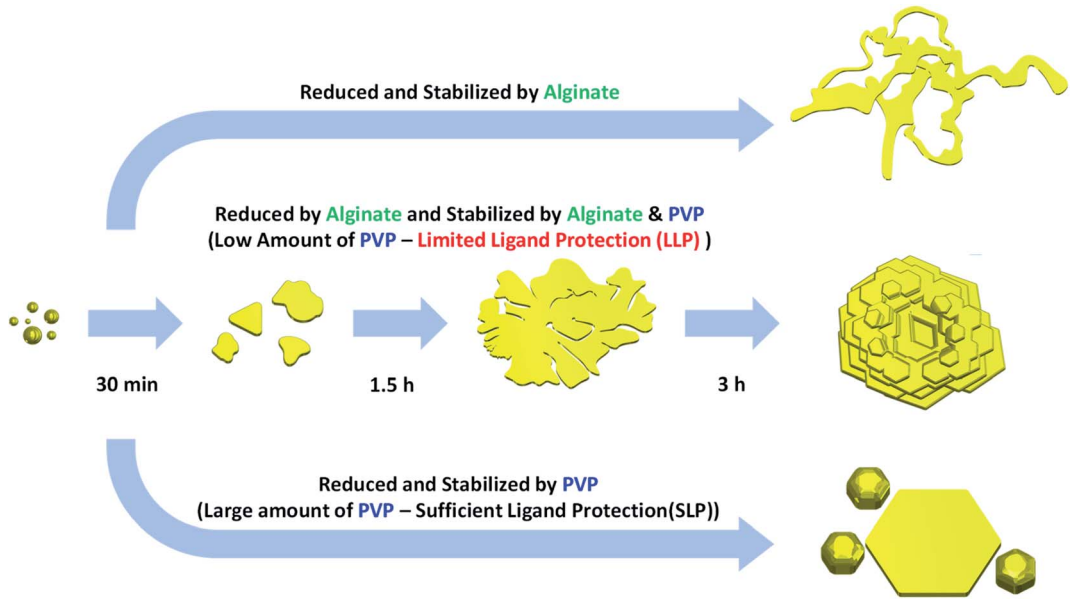

Fig. 5 Schematic of the shape changes of Au nanocrystals depending on the amount of PVP, which was used as a capping ligand in the present study. The rose-shaped Au nanostructures can be formed in the special reaction region corresponding to limited ligand protection (LLP).

The nanoplates with abundant edges and tips observed in Fig. 3(b) and (c) exhibit irregular and asymmetric shapes; however, their thickness is uniform. Given their structural characteristics, these nanoplates are not expected to have formed through the normal growth process based on Ostwald ripening.[62] The secondary structure of nanoplates with abundant edges and sharp tips rich in single particles is expected to form by fusion of the initially formed primary nanoplates together along the side surfaces through oriented attachment.[63] Close examination of the morphology of a single large Au nanoplate (Fig. S6†) confirms the nanoplate growth mechanism through oriented attachment. Several lines observed on the top and bottom surfaces of large nanoplates are attributed to incomplete fusion of small nanoplates. In addition, the large nanoplate shows overlapping structures, which cannot be explained by a growth mechanism based on Ostwald ripening.

Under kinetically controlled reaction conditions based on a single-step synthesis method, the lateral growth of nanoplates tends to stop when the nanoplates reach a certain size.[64] As far as we know, nanoplates synthesized by conventional single-step solution-phase synthesis pathways have rarely grown to more than 500 nm in lateral size.[65] In addition, the amount of PVP is not sufficient to effectively cap the top and bottom {111} surfaces of the nanoplates in the LLP reaction region; consequently, the newly generated Au nanoplates stack on the surface of the existing large nanoparticles, forming layered structures. As the number of stacked nanoplates increases, the particles grow vertically to form rose-shaped nanostructures.

To investigate the effect of the concentration of the precursor, $HAuCl_4$, on the growth of the Au nanostructures, an identical experiment was conducted by adjusting the concentration of the $HAuCl_4$ precursor from 0.38 mM to 1.25 mM. Fig. 6(a) shows a TEM image of Au nanocrystals formed when the $HAuCl_4$ concentration was 0.38 mM. At this low concentration of $HAuCl_4$, the amount of reduced Au atoms was insufficient, resulting in the growth of small nanocrystals into small tadpole-like structures. When the concentration of $HAuCl_4$ was increased to 0.63 mM, thin plate-shaped particles were observed (Fig. 6(b)). The increase in concentration of $HAuCl_4$ led to the synthesis of particles larger than those obtained under the 0.38 mM condition; in the 0.63 mM case, nanoplates similar to those observed in the initial growth stage of rose-shaped

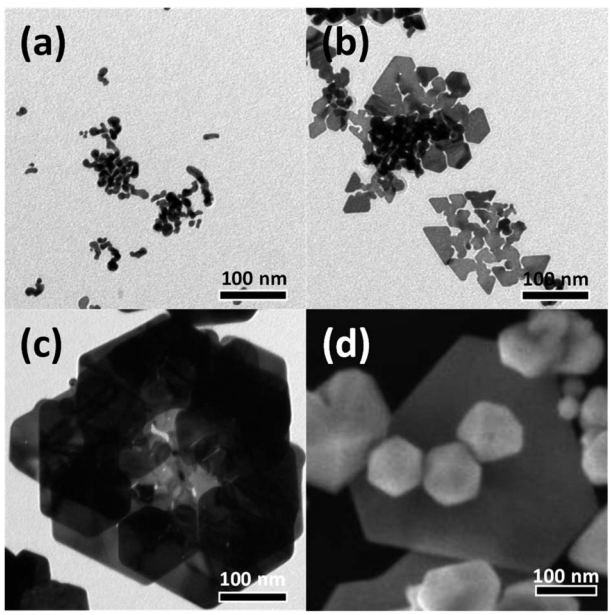

Fig. 6 (a)–(c) TEM and (d) SEM images of Au nanostructures synthesized using various concentrations of $HAuCl_4$: (a) 0.38 mM, (b) 0.63 mM, (c) 0.88 mM, and (d) 1.25 mM.

© 2021 The Author(s). Published by the Royal Society of Chemistry

Open Access Article. Published on 26 October 2021. Downloaded on 1/16/2025 9:05:36 AM.
This article is licensed under a Creative Commons Attribution-NonCommercial 3.0 Unported Licence.

nanoparticles were obtained. However, because the amount of Au atoms produced was still insufficient, single-layered structures rather than 3D stacked structures were formed. When the concentration of $HAuCl_4$ was increased to 1.25 mM, most of the particles were multiply twinned particles; a few hexagonal plate-shaped particles were also observed. When the concentration of $HAuCl_4$ was increased, the amount of reduced Au atoms increased; thus, multiply twinned particles with thermodynamically preferred structures were generated (Fig. 6(d)). In the present study, the optimal concentration of $HAuCl_4$ for synthesizing the rose-shaped nanostructures was found to be 0.88 mM.

Catalytic performance of rose-shaped Au nanostructures

Au nanocrystals have been widely used as catalysts because of their greatly enhanced stability and high catalytic activity.[66] Catalytic reactions that use water instead of toxic organic solvents have great environmental advantages.[34,35] Because the rose-shaped Au nanostructures synthesized in the present study are stabilized by alginate and PVP and dispersed in water, eco-friendly catalytic reaction experiments could be performed. In addition, because the rose-shaped Au nanostructures have an average particle size of almost 500 nm and a three-dimensionally stacked structure, they can be easily separated from the reaction mixture through simple precipitation or centrifugation. Accordingly, excellent recovery and recyclability of the catalysts can be obtained after the catalytic reaction is completed.

The synthesized rose-shaped Au nanostructures were used as catalysts in the hydrogenation of 4-NP to 4-AP by $NaBH_4$. When $NaBH_4$ was added to a 4-NP aqueous solution, the absorption peak at 317 nm shifted to 398 nm, confirming that 4-NP was changed to 4-nitrophenolate ion (Fig. 7(a)).[67] The absorption peak of 4-AP appeared at 305 nm in the absorption spectrum. Spontaneous reduction of 4-NP to 4-AP is possible in the presence of $NaBH_4$; however, this reaction requires several days.[68] The addition of a small amount of catalyst can increase the speed of electron transfer from the $NaBH_4$ to the 4-nitrophenolate ions, thereby reducing the time required for the reduction reaction. In the reduction process of 4-NP, Au nanocrystals adsorb hydrogen species generated by $NaBH_4$, along with 4-nitrophenolate ions, which facilitates electron transfer.[69] Fig. 7(b) shows the UV-Vis spectra recorded every 10 s after the addition of the rose-shaped Au nanostructures to an aqueous solution containing $NaBH_4$ and 4-NP. The intensity of the absorption peak at 398 nm gradually decreased over time, and, after 210 s, its intensity was almost zero. Simultaneously, an absorption peak at ~305 nm appeared, indicating that the hydrogenation reaction was successful. Because the concentration of $NaBH_4$ was excessive compared with that of 4-NP, the reaction rate was not dependent on the concentration of $NaBH_4$, thereby allowing the reaction rate constant could be calculated

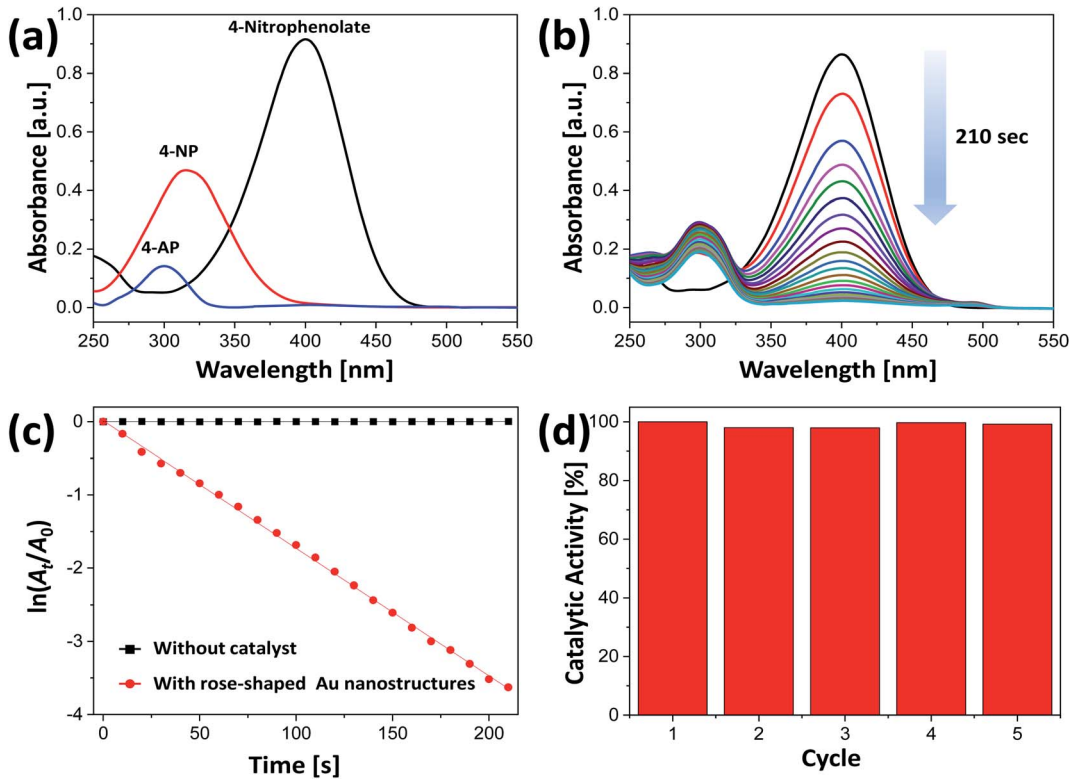

Fig. 7 Catalytic activity test of the rose-shaped Au nanostructures; the test was based on the catalytic hydrogenation of 4-nitrophenol (4-NP) to 4-aminophenol (4-AP) by $NaBH_4$. (a) UV-Vis spectra of 4-NP (red), 4-nitrophenolate ion (black), and 4-AP (blue). (b) UV-Vis spectral changes during the catalytic reduction for 210 s in the presence of the rose-shaped Au nanostructures. (c) Plot of $\ln(A_t/A_0)$ as a function of the reaction time t. (d) Reusability of the Au nanoparticles as catalysts for the hydrogenation of 4-NP.

© 2021 The Author(s). Published by the Royal Society of Chemistry

Open Access Article. Published on 26 October 2021. Downloaded on 1/16/2025 9:05:36 AM.
This article is licensed under a Creative Commons Attribution-NonCommercial 3.0 Unported Licence.

on the basis of the pseudo-first-order reaction equation.[70,71] Fig. 7(c) shows that a plot of $\ln(A_t/A_0)$ *vs.* time is linear, where A_0 and A_t are the absorbances at times 0 and t, respectively. The reaction rate constant (k) of the rose-shaped Au nanostructures used in the present study was calculated to be 17.4×10^{-3} s^{-1}. The absorption spectra acquired after 210 s of the hydrogenation reaction conducted with only $NaBH_4$ and 4-NP (*i.e.*, without the Au nanostructures) showed no change over time, indicating that the hydrogenation reaction was slow in the absence of the Au nanostructures (Fig. S6†).

The recycling and reuse of catalysts without incurring a substantial loss of activity are critical factors in assessing their industrial and practical effectiveness.[72,73] The rose-shaped Au nanostructures synthesized in the present study were easily separated from the reaction solution by centrifugation after the catalytic reaction because they were several hundred nanometers in size and had three-dimensionally stacked structures. Recyclability and reusability were evaluated by repeatedly using the same catalysts in the reduction of 4-NP to 4-AP. As evident in Fig. 7(d), the conversion rate of 4-NP did not substantially decrease compared with its initial conversion rate, even after five uses, indicating excellent reusability and stability of the catalyst.

Using the activity parameter (κ) obtained by dividing the rate constant (k) by the total mass (m) of the catalyst used, we compared the catalytic activity of the rose-shaped Au nanostructures with the activities of recently reported catalysts.[44,45,74] The κ-value of the rose-shaped Au nanostructures was calculated to be 290 s^{-1} g^{-1}, which is substantially greater than the values for other noble-metal-based catalysts (Table S1†). The high catalytic activity of the rose-shaped Au nanostructures synthesized in the present study is attributable to their unique structure. The rose-shaped nanostructures with a 3D hierarchically layered structure have a large specific surface area and abundant active sites such as sharp tips, edges, and steps, which tend to result in extremely high catalytic activity.[75,76]

Conclusions

A one-pot completely green method for synthesizing rose-shaped Au nanostructures at room temperature was developed. In this method, water was used as a reaction medium in all of the reactions. Na-alginate, a bio-derived polymer, served as a reducing and stabilizing agent, and PVP, a nontoxic and biocompatible polymer, acted as a capping ligand. According to the mechanism proposed in the present study, the amount of PVP in the reaction mixture strongly affected the shape of the obtained Au nanostructures. In the special LLP reaction region, irregular and asymmetric large Au nanoplates with abundant edges and sharp tips were first formed *via* oriented attachment; the newly created Au nanoplates continued to grow on the surface of the as-synthesized large nanoplates, forming rose-shaped nanostructures. Because the rose-shaped Au nanostructures were large, stable, and featured abundant active sites such as sharp tips and edges, they could be used as efficient environmentally friendly catalysts without requiring a supporting material. They showed outstanding catalytic activity, high stability, and excellent recyclability when used as a catalyst for the hydrogenation of 4-NP to 4-AP by $NaBH_4$. This study has not only established an eco-friendly method for synthesizing Au nanostructures with unique three-dimensional hierarchical structures, but also provides an approach that can be used to develop an environmentally benign catalyst with excellent catalytic performance and reusability.

Author contributions

Jae Hwan Jeong: conceptualization, methodology, investigation, writing – original draft. Astrini Pradyasti: methodology, investigation. Hyeonbo Shim: methodology, investigation. Hee-Chul Woo: validation, investigation. Mun Ho Kim: conceptualization, methodology, validation, investigation, resource, writing – review & editing, supervision, project administration, funding acquisition.

Conflicts of interest

The authors declare that they have no known competing financial interests or personal relationships that could have appeared to influence the work reported in this paper.

Acknowledgements

This research was supported by the National Research Foundation of Korea (NRF) grant funded by the Korea government (MSIT) (No. 2017R1E1A01074445). This work was also supported by the Korea Institute of Energy Technology Evaluation and Planning (KETEP) and the Ministry of Trade, Industry & Energy (MOTIE) of the Republic of Korea (No. 20194010201840).

References

1 T.-H. Yang, Y. Shi, A. Janssen and Y. Xia, *Angew. Chem., Int. Ed.*, 2020, **59**, 15378–15401.
2 M. Grzelczak, J. Pérez-Juste, P. Mulvaney and L. M. Liz-Marzán, *Chem. Soc. Rev.*, 2008, **37**, 1783–1791.
3 W. Lu, X. Cui, T. H. Chow, L. Shao, H. Wang, H. Chen and J. Wang, *Nanoscale*, 2019, **11**, 9641–9653.
4 Z. Chen, T. Balankura, K. A. Fichthorn and R. M. Rioux, *ACS Nano*, 2019, **13**, 1849–1860.
5 K. I. Requejo, A. V. Liopo and E. R. Zubarev, *Langmuir*, 2020, **36**, 3758–3769.
6 Q. Zhai, Y. Wang, S. Gong, Y. Ling, L. W. Yap, Y. Liu, J. Wang, G. P. Simon and W. Cheng, *Anal. Chem.*, 2018, **90**, 13498–13505.
7 L. Yan, J. Mu, P. Ma, Q. Li, P. Yin, X. Liu, Y. Cai, H. Yu, J. Liu, G. Wang and A. Liu, *Chem. Commun.*, 2021, **57**, 1133–1136.
8 G. Zhang, Y. Ma, M. Li, S. Ren, X. Fu, H. Huang and Y. Zheng, *Langmuir*, 2021, **37**, 4227–4235.
9 Y. Li, M. Zhai and H. Xu, *Appl. Surf. Sci.*, 2019, **498**, 143864.
10 C. Liu, L. Tan, L. Li, J. Dong and W. Qian, *CrystEngComm*, 2017, **19**, 3233–3236.
11 J. Yoon, H. J. Jang, I. Jung and S. Park, *Nanoscale*, 2017, **9**, 7708–7713.

© 2021 The Author(s). Published by the Royal Society of Chemistry

Open Access Article. Published on 26 October 2021. Downloaded on 1/16/2025 9:05:36 AM.
This article is licensed under a Creative Commons Attribution-NonCommercial 3.0 Unported Licence.

12 L.-X. Chen, J.-J. Lv, A.-J. Wang, H. Huang and J.-J. Feng, *Sens. Actuators, B*, 2016, **222**, 937–944.
13 S. A. Lone and K. K. Sadhu, *Bioconjugate Chem.*, 2019, **30**, 1781–1787.
14 C. Y. Song, B. Y. Yang, W. Q. Chen, Y. X. Dou, Y. J. Yang, N. Zhou and L. H. Wang, *J. Mater. Chem. B*, 2016, **4**, 7112–7118.
15 S.-J. Park, M.-L. Seol, S.-B. Jeon, D. Kim, D. Lee and Y.-K. Choi, *Sci. Rep.*, 2015, **5**, 13866.
16 Z. Guo, Y. Zhang, A. Xu, M. Wang, L. Huang, K. Xu and N. Gu, *J. Phys. Chem. C*, 2008, **112**, 12638–12645.
17 V. M. Kariuki, J. C. Hoffmeier, I. Yazgan and O. A. Sadik, *Nanoscale*, 2017, **9**, 8330–8340.
18 D. Borah, M. Hazarika, P. Tailor, A. R. Silva, B. Chetia, G. Singaravelu and P. Das, *Appl. Nanosci.*, 2018, **8**, 241–253.
19 I. C. De Freitas, L. S. Parreira, E. C. M. Barbosa, B. A. Novaes, T. Mou, T. V. Alves, J. Quiroz, Y.-C. Wang, T. J. Slater, A. Thomas, B. Wang, S. J. Haigh and P. H. C. Camargo, *Nanoscale*, 2020, **12**, 12281–12291.
20 C. Chen, D. Y. W. Ng and T. Weil, *Mater. Chem. Front.*, 2019, **3**, 1449–1453.
21 S. Ye, F. Benz, M. C. Wheeler, J. Oram, J. J. Baumberg, O. Cespedes, H. K. Christenson, P. L. Coletta, L. J. C. Jeuken, A. F. Markham, K. Critchley and S. D. Evans, *Nanoscale*, 2016, **8**, 14932–14942.
22 Z. Wang, Y. Li, H. Yu, Y. Xu, H. Xue, X. Li, H. Wang and L. Wang, *ChemSusChem*, 2018, **11**, 3480–3485.
23 M. Pradhan, J. Chowdhury, S. Sarkar, A. K. Sinha and T. Pal, *J. Phys. Chem. C*, 2012, **116**, 24301–24313.
24 S. A. Lone and K. K. Sadhu, *ChemPlusChem*, 2019, **84**, 112–118.
25 C. Kuttner, M. Mayer, M. Dulle, A. Moscoso, J. M. López-Romero, S. Förster, A. Fery, J. Pérez-Juste and R. Contreras-Cáceres, *ACS Appl. Mater. Interfaces*, 2018, **10**, 11152–11163.
26 F. J. Osonga, P. Le, D. Luther, L. Sakhaee and O. A. Sadik, *Environ. Sci.: Nano*, 2018, **5**, 917–932.
27 B. Bhattarai, Y. Zaker and T. P. Bigioni, *Curr. Opin. Green Sustain. Chem.*, 2018, **12**, 91–100.
28 N. A. I. Md Ishak, S. K. Kamarudin and S. N. Timmiati, *Mater. Res. Express*, 2019, **6**, 112004.
29 Y. N. Wijaya, J. Kim, W. M. Choi, S. H. Park and M. H. Kim, *Nanoscale*, 2017, **9**, 11705–11712.
30 J. H. Jeong, H.-C. Woo and M. H. Kim, *RSC Adv.*, 2021, **11**, 22826–22834.
31 W. Leng, P. Pati and P. J. Vikesland, *Environ. Sci.: Nano*, 2015, **2**, 440–453.
32 R. Prabhu, T. Jeevananda, K. R. Reddy and A. V. Raghu, *Mater. Sci. Energy Technol.*, 2021, **4**, 107–112.
33 J. L. Hodala, D. J. Moon, K. R. Reddy, C. V. Reddy, T. N. Kumar, M. I. Ahamed and A. V. Raghu, *Int. J. Hydrogen Energy*, 2021, **46**, 3289–3301.
34 X. Kong, Y. Zhu, Z. Fang, J. A. Kozinski, I. S. Butler, L. Xu, H. Song and X. Wei, *Green Chem.*, 2018, **20**, 3657–3682.
35 T. Kitanosono, K. Masuda, P. Xu and S. Kobayashi, *Chem. Rev.*, 2018, **118**, 679–746.
36 M. A. Ahsan, V. Jabbari, A. A. El-Gendy, M. L. Curry and J. C. Noveron, *Appl. Surf. Sci.*, 2019, **497**, 143608.
37 K. Kannan, D. Radhika, A. S. Nesaraj, K. Kumar Sadasivuni, K. R. Reddy, D. Kasai and A. V. Raghu, *Mater. Sci. Energy Technol.*, 2020, **3**, 853–861.
38 S. R. Manippady, A. Singh, B. M. Basavaraja, A. K. Samal, S. Srivastava and M. Saxena, *ACS Appl. Nano Mater.*, 2020, **3**, 1571–1582.
39 J.-G. You, C. Shanmugam, Y.-W. Liu, C.-J. Yu and W.-L. Tseng, *J. Hazard. Mater.*, 2017, **324**, 420–427.
40 A. S. Hashimi, M. A. N. M. Nohan, S. X. Chin, S. Zakaria and C. H. Chia, *Nanomaterials*, 2019, **9**, 936.
41 N. Meng, S. Zhang, Y. Zhou, W. Nie and P. Chen, *RSC Adv.*, 2015, **5**, 70968–70971.
42 J. Strachan, C. Barnett, A. F. Masters and T. Maschmeyer, *ACS Catal.*, 2020, **10**, 5516–5521.
43 F. Ali, S. B. Khan, T. Kamal, K. A. Alamry and A. M. Asiri, *Sci. Rep.*, 2018, **8**, 6260.
44 D. H. Kim, J. H. Jeong, H.-C. Woo and M. H. Kim, *Chem. Eng. J.*, 2021, **420**, 127628.
45 D. H. Kim, H.-C. Woo and M. H. Kim, *Langmuir*, 2019, **35**, 13700–13710.
46 S. H. Kim, H.-C. Woo and M. H. Kim, *Anal. Chim. Acta*, 2020, **1131**, 80–89.
47 S. H. Kim, J. H. Jeong, H. Shim, H.-C. Woo, K. B. C. Imani, J. Yoon, J. H. Jeong and M. H. Kim, *Smart Mater. Struct.*, 2021, **30**, 075014.
48 K. M. Koczkur, S. Mourdikoudis, L. Polavarapu and S. E. Skrabalak, *Dalton Trans.*, 2015, **44**, 17883–17905.
49 Y. Ma and L.-Y. L. Yung, *Langmuir*, 2016, **32**, 7854–7859.
50 J. Kim, S. W. Lee, M. H. Kim and O. O. Park, *ACS Appl. Mater. Interfaces*, 2018, **10**, 39134–39143.
51 S. Ye, A. P. Brown, A. C. Stammers, N. H. Thomson, J. Wen, L. Roach, R. J. Bushby, P. L. Coletta, K. Critchley, S. D. Connell, A. F. Markham, R. Brydson and S. D. Evans, *Adv. Sci.*, 2019, **6**, 1900911.
52 W. Xin, I. M. De Rosa, P. Ye, J. Severino, C. Li, X. Yin, M. S. Goorsky, L. Carlson and J.-M. Yang, *Nanoscale*, 2018, **10**, 2764–2773.
53 A. Pradyasti, J. H. Jeong, S. H. Kim and M. H. Kim, *J. Alloys Compd.*, 2021, **865**, 158812.
54 J. Xie, Q. Zhang, J. Y. Lee and D. I. C. Wang, *ACS Nano*, 2008, **2**, 2473–2480.
55 A. Narayanaswamy, H. Xu, N. Pradhan, M. Kim and X. Peng, *J. Am. Chem. Soc.*, 2006, **128**, 10310–10319.
56 L. Liu, Z. Gao, B. Jiang, Y. Bai, W. Wang and Y. Yin, *Nano Lett.*, 2018, **18**, 5312–5318.
57 A. Narayanaswamy, H. Xu, N. Pradhan and X. Peng, *Angew. Chem., Int. Ed.*, 2006, **45**, 5361–5364.
58 G. Guan, K. Y. Win, X. Yao, W. Yang and M.-Y. Han, *Adv. Healthcare Mater.*, 2021, **10**, 2001158.
59 Y. Xiong, I. Washio, J. Chen, H. Cai, Z.-Y. Li and Y. Xia, *Langmuir*, 2006, **22**, 8563–8570.
60 H. Wang, S. Zhou, K. D. Gilroy, Z. Cai and Y. Xia, *Nano Today*, 2017, **15**, 121–144.
61 T. Yu, Z. Wu and W. S. Kim, *RSC Adv.*, 2014, **4**, 37516–37521.
62 M. H. Kim, D. K. Yoon and S. H. Im, *RSC Adv.*, 2015, **5**, 14266–14272.

Open Access Article. Published on 26 October 2021. Downloaded on 1/16/2025 9:05:36 AM.
This article is licensed under a Creative Commons Attribution-NonCommercial 3.0 Unported Licence.

63 A. Shahzad, S. H. Bhang, E. Jung, W.-S. Kim and T. Yu, *J. Materiomics*, 2018, **4**, 121–128.
64 Y. M. Park, B. G. Lee, J. Il Weon and M. H. Kim, *RSC Adv.*, 2016, **6**, 95768–95773.
65 J. Zeng, X. Xia, M. Rycenga, P. Henneghan, Q. Li and Y. Xia, *Angew. Chem., Int. Ed.*, 2011, **50**, 244–249.
66 J. Zeng, Q. Zhang, J. Chen and Y. Xia, *Nano Lett.*, 2010, **10**, 30–35.
67 S. H. Park, J. Kim, S. H. Hur, D. H. Kim and M. H. Kim, *Chem. Eng. J.*, 2018, **348**, 46–56.
68 M. Zhang, X. Su, L. Ma, A. Khan, L. Wang, J. Wang, A. S. Maloletnev and C. Yang, *J. Hazard. Mater.*, 2021, **403**, 123870.
69 P. Suchomel, L. Kvitek, R. Prucek, A. Panacek, A. Halder, S. Vajda and R. Zboril, *Sci. Rep.*, 2018, **8**, 4589.
70 Y. Zhang, Y. Xia, S. Yan, J. Han, Y. Chen, W. Zhai and Z. Gao, *Dalton Trans.*, 2018, **47**, 17461–17468.
71 A. A. L. Ahmad, S. Panicker, M. M. Chehimi, M. Monge, J. M. Lopez-De-Luzuriaga, A. A. Mohamed, A. E. Bruce and M. R. M. Bruce, *Catal. Sci. Technol.*, 2019, **9**, 6059–6071.
72 Y. Kou, T. Wu, G. Xing, X. Huang and D. Han, *Nanotechnology*, 2020, **31**, 225701.
73 M. Miceli, P. Frontera, A. Macario and A. Malara, *Catalysts*, 2021, **11**, 591.
74 C. Kästner and A. F. Thünemann, *Langmuir*, 2016, **32**, 7383–7391.
75 H. Zhu, M. Du, M. Zhang, M. Zou, T. Yang, Y. Fu and J. Yao, *J. Mater. Chem. A*, 2014, **2**, 7680–7685.
76 T. H. Yang, J. Ahn, S. Shi, P. Wang, R. Gao and D. Qin, *Chem. Rev.*, 2021, **121**, 796–833.

© 2021 The Author(s). Published by the Royal Society of Chemistry